ENERGY STORAGE-BASED MICROGRID INTEGRATED WITH UTILITY GRID FOR FUZZY CONTROLLED DUAL MODE OPERATION OF HYBRID RENEWABLE ENERGY SOURCES

Ch. Sajan [1], B. Madan [2], B. Poojitha[3], P. Pravalika[4], B. Akhil [5]

[1]Associate Professor, Department of EEE, Jyothishmathi Institute of Technology and Science, Nustulapur, Karimnagar, Telangana, India

[2,3,4,5] UG students, Department of EEE, Jyothishmathi Institute of Technology and Science, Nustulapur, Karimnagar, Telangana, India

Abstract

The integrated operation of the microgrid with assistance from the utility grid provides both continuous power availability and electrification of the rural areas. The application of Renewable energy sources, such as wind and solar photovoltaic (PV) arrays, support the grid and lower electricity costs. In this paper, a dual mode transfer scheme is used, which allows the control to switch from the present control mode to an independent functioning mode in the event of a power outage or grid failure. The signal sent to the static transfer switches (STS) determines when the operational modes begin. Reducing the renewable intermittent nature of wind and solar PV arrays is made possible in large part by the microgrid's energy storage and grid link. Then By regulating local load support, the improvement in power quality (PQ) as well as energy security and sufficiency are perceived. In the grid-connected mode of operation, or current control, the bias compensated improved affine projection like (BC-IAPL) adaptive filter is used; in the standalone mode, or voltage control, the modified proportional resonant (MPR) controller is aided by dual modified generalized integrator-based phase locked loop (DMGI-PLL). The cost of mechanical sensors is decreased by using a modified sensor less technique to estimate the wind generator's speed and rotor position. A detailed understanding of the microgrid's cooperative behavior is established.

Keywords—FUZZY logic controller; AC-IAPL adaptive filter; PR controller modification; microgrid; power quality; dual mode operation and DMGI-PLL.

1. INTRODUCTION

Energy generation has progressed over time, both in terms of supplies and methods. All existing approaches and technologies have praised the clean power and absence of carbon emissions produced by energy generation from renewable energy sources (RESs). Renewable energy sources (RESs) provide several advantages, including lowering power costs, improving power reliability and resilience, and bringing electricity to remote regions that do not have grid connectivity or AC distribution networks [1]. For these so-called "microgrid" systems to function, they must be able to run independently while simultaneously connecting to the larger grid. Another crucial consideration is the reliability and unpredictability of renewable energy sources, including PV arrays for solar and wind power [2-3]. Predicting the microgrid's dependable and problem-free functioning becomes more challenging. Battery energy storage (BES) is used to adapt to changes in load

demands and power generation irregularities. Using BES as a subordinate to mitigate power fluctuations is highly beneficial for isolated microgrids. It may take on the role of a generator or a load depending on whether it is being charged or discharged. Ensuring that electricity is always accessible requires powering key loads, even in the event of a grid outage. In the case of a power loss, it provides backup power and greatly enhances the system's stability and dependability. Flexible microgrids that can function in either the large or small grid integrated and independent modes can make the most of their capacity by taking into account the advantages of RESs connected to BES. A microgrid's dependability stems from its four operation modes: grid integrated, standalone, seamless grid to island, and islanded to grid integrated. The renewable power generation units may adjust the voltage, output frequency, reactive and active powers, and other parameters involved in these activities through the power electronic interface. By connecting to the microgrid, controllers of voltage source converters (VSCs) ensure that all operating modes can fulfil the demand for local loads. Rapid response, low overload, and low inertia are some of the advantages offered by VSCs [4]. Some electrical policymakers, however, continue to rely on the synchronization requirements laid forth in the IEEE-1547-2018 standard [5]. Over the last ten years, an abundance of research has focused on microgrid mode transfer control. For a smooth transition from grid isolation to grid integration, the load voltage must be in harmony with the utility after being linked with microgrid operations. Using phase-locked loops (PLLs), one may regulate synchronization and track the load-to-utility grid voltage difference [6]. While PLLs function dependably in an evenly distributed grid, their behaviour becomes very unpredictable in an unbalanced or distorted grid. Consequently, research on enhanced PLLs is also continuing. Yazdani et al [7]. Have provided the VSC controller for both grid-connected and independent modes of operation. Whatever the case may be, reports have surfaced of skewed load currents and voltages and performance spikes during mode changeover. In [8], the authors used an indirect current approach to provide a smooth transition and precise control. We carefully measure the phase angle on each of the around eighteen synchronization and resynchronization cycles. Providing dependable control for grid synchronization, [9] carefully monitors the transfer process while reducing voltage and current spikes. Prior research on synchronization has mostly disregarded the IEEE-519 power quality indicators [10]. Among the components examined in this research are a wind-responsive synchronous generator (SG), a battery energy system (BES) linked to the DC link by a bidirectional buck-boost DC-DC converter, and a PV array with a single stage of integration. Charging and draining the battery are better managed when the BES and BDC converter are used together. The longer the run duration, the less capacity the battery needs compared to connecting it directly to the DC socket. In cases when the second harmonic is too powerful, the BDC is responsible for shielding the DC connection from the BES faults [11]. Solar PV modules in a single-stage array are more efficient than those in a two-stage system. In spite of this, the system's4 small size, simplicity, low cost, and little losses allow for a wide working range. Energy harvesting systems that employ wind turbines and solar PV arrays calculate the MPP using the P&O approach [13]. An off-grid detection non-detection zone, denoted by the power difference, is present. The NDZ condition cannot be achieved when the voltage, frequency, and phase are perfectly synchronized. Big power plants use active and passive islanding detection techniques to stay out of NDZ. The microgrid's power quality can be improved by intentionally introducing harmonics. This study investigates the viability of low-power residential microgrids in fulfilling the demands of families by using a passive islanding detection technique. As a result of synchronization/static transfer switches (STS), it is feasible to disconnect

from and rejoin to the AC distribution grid. In such cases, a voltage-, phase-angle-, and frequency-aware smooth mode shifting controller is used. When the current or voltage drops below a certain threshold, the STS switch will automatically go to voltage/current mode, where you may regulate both variables. In order to make the microgrid work and transition modes, this paper investigates the five main controllers.

• Machine-side converters (MSCs) for controlling the output of wind turbine generators: Two VSCs are coupled utilizing back-to-back (BTB) technology to produce wind at varied speeds. Since mechanical and electrical powers are entirely distinct, there will be zero power fluctuations caused by differences in wind speed. With a tweak to the back-EMF sensor-less speed estimate approach, we can find out where the synchronous generator is and how fast it's going. By connecting to the terminals of the synchronous generators, the unity power factor (UPF) may be controlled [14]. The wind PPP makes use of the time-tested perturb-and-observe technique [12]. Signals are sent to the machine side converter (MSC) by the integrated control.

• Supervision present state of this LSC: the BC-IAPL filter, which stands for bias-corrected improved affine projection is composed of adaptive filters. Which is employed to generate the switching pulses for the LSC. One area where it has been used before is to reduce noise in picture and signal processing [15]. It may be used to determine the load's basic mass. The controller's computational load is reduced, and noise rejection is increased. Under impulsive noise inputs, convergence and performance are both improved.

• The LSC voltage control is accomplished with the use of an MPR controller, which modifies the original design. More control over sinusoidal signals is available with the MPR controller [16]. A DMGI-PLL, or dual modified generalized integrator phase locked loop [17], helps fix microgrid tracking problems brought on by frequency variations. The DMGI-PLL communicates with the MPR controller to send the estimated frequency. When compared to traditional PR controllers, the results demonstrate an improvement in performance. When the microgrid experiences frequency shifts, non-adaptive filters will not function properly.

• Using the state space technique, the two-mode operation may be controlled. The STS switch is set up to cycle from 1 to 0/0 to 1 in the event that there is a voltage, phase angle, or frequency differential between the grid and the load [18]. It stands for the utility reconnection method of operation, which is also called islanding or the STS switch's activation and deactivation. The microgrid transitions from regulating current and voltage to all three of these parameters when the recorded voltage, frequency, and phase angle surpass these limits, which are ±&V_R V, ±&f_R Hz, '±& (°). The DMGI-PLL architecture continues to provide the predicted grid and load voltages, phases, frequencies, and voltages regardless of changes in the microgrid conditions.

• The BDC converter shields the BES from DC that is dominated by second harmonics. connection ripples and significantly lowers the battery rating in a BDC-controlled BES. When these controls are coordinated, the microgrid may transition between using the grid and not using the grid with little effort.

2. MICROGRID STRUCTURE

Figure 1 shows the design of the microgrid. A direct current motor that simulates a wind turbine is employed to provide power to the wind turbine from SG. Two VSCs, the MSC and the LSC, are linked in a sequential way; their rates of wind power generation are different. A BES and a PV array with a single stage of solar panels are connected through the DC connection. In this architecture, the STS are shown operating as synchronization switches. Their solution allows for the seamless connection and disconnection of the grid from

the microgrid. When the diode bridge rectifier's output is 6yconnected to the RL components—a resistor and an inductor—local loads are realized. Harmonics, produced by a non-linear load, decrease power quality and alter grid current. Interface inductors and RC filters remove the switching harmonics and current.

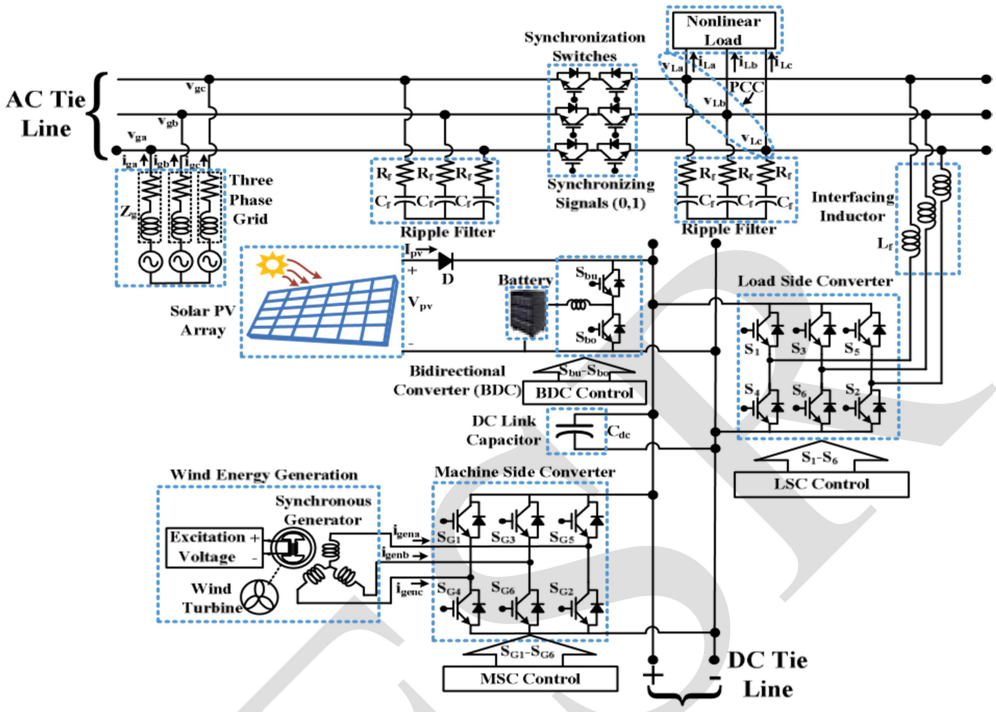

Fig. 1 Microgrid Configuration

3. CONTROL METHODOLOGY

One of these modes is the microgrid control, which is used for islanding or utility reconnection. Wind turbine and photovoltaic array performance is mostly dependent on solar insolation and wind speed. As the microgrid's total power production and load demand fluctuate, the battery's charging and discharging functions adapt accordingly. The controller that changes modes switches between voltage/ present management of the flow and current/voltage

Chapter One: MSC Administration See Figure 2 for an illustration of the MSC gate controller. In order to control the wind turbine generator, it is necessary to measure the current components of the rotor's magnetic flux ($I_{d\ ref}$) and torque ($I_{q\ ref}$).

Assessment of $I_{q\ ref}$

In order to determine the speed error, we compare the cited work reference for SG speed provided by the P&O PPP control system to the standard ω_{genest}, the speed PI controller then receives it. Elements that govern the wind PPP approach are [12],

$$\omega_{gen\,ref}(k) = \omega_{gen\,ref}(k-1) + \Delta\omega_{gen};$$

$$if \begin{Bmatrix} \Delta P_{wind}>0 \text{ and } \Delta\omega_{gen\,est}>0 \\ \Delta P_{wind}<0 \text{ and } \Delta\omega_{gen\,est}<0 \end{Bmatrix} \quad (1)$$

$$\omega_{gen\,ref}(k) = \omega_{gen\,ref}(k-1) - \Delta\omega_{gen\,ref};$$

$$if \begin{Bmatrix} \Delta P_{wind}>0 \text{ and } \Delta\omega_{gen\ est}<0 \\ \Delta P_{wind}<0 \text{ and } \Delta\omega_{gen\ est}>0 \end{Bmatrix} \quad (2)$$

In order to rectify this oversight, we include equations for both the speed PI controller and its by-product, the $I_{q\ ref}$ component.

$$\omega_{error}(k) = \omega_{gen\ ref}(k) - \omega_{gen\ ref}(k) \quad (3)$$

$$I_{q\ ref}(k) = I_{q\ ref}(k-1) + k_{isg}\{\omega_{error}(k) - \omega_{error}(k-1)\} + k_{psg}\{\omega_{error}(k)\} \quad (4)$$

1) Calculation of $I_{d\ ref}$

The creation of $I_{d\text{-}ref}$ is contingent upon the synchronous generator terminals maintaining the unit power factor (UPF). This rule is determined by the formula [12],

$$I_{d\ ref} = \frac{\lambda_r - \sqrt{\lambda^2 r - 4L_d L_q i^2 q}}{2L_d} \quad (5)$$

where *r stands for the r-value, L_d for the rotor flux linkage, and L_q for the d-axes inductances. The reference elements ($I_{gena\ ref}$, $I_{genb\ ref}$, and $I_{genc\ ref}$) may be obtained by applying the dq0 to abc transformation to I_{qref} and I_{dref} as well. The switching generator receives the output when the reference and sensing currents are equal, and then it generates the MSC switching pulses (SSG1 through SSG6).

3.1. BC-IAPL Adaptive Filter for Current Control of LSC

With grid availability guaranteed, the control now in use for LSC may be shown in Figure 3. Its many components work in harmony with one another. This section will provide an in-depth analysis of each subject.

1)Assessment of Unit Templates and PCC Terminal Voltage Using two measured line voltages, the grid's phase voltages are assessed.

$$v_{ga} = \left(\frac{2v_{gab} + v_{gbc}}{3}\right); v_{ga}\left[\frac{-v_{gab} + v_{gbc}}{3}\right];$$

$$v_{gc} = \left(\frac{-v_{gab} - 2v_{gbc}}{3}\right) \quad (6)$$

The voltage at the PCC terminal is measured as

$$V_t = \sqrt{\frac{2}{3}\left(v^2{}_{ga} + v^2{}_{gb} + v^2{}_{gc}\right)} \quad (7)$$

It is anticipated that the unit templates are, based on (1) and (2),

$$u_a = \frac{v_{ga}}{V_t}; v_{gb} = \frac{v_{gb}}{V_t}; u_c = \frac{v_{gc}}{V_t} \quad (8)$$

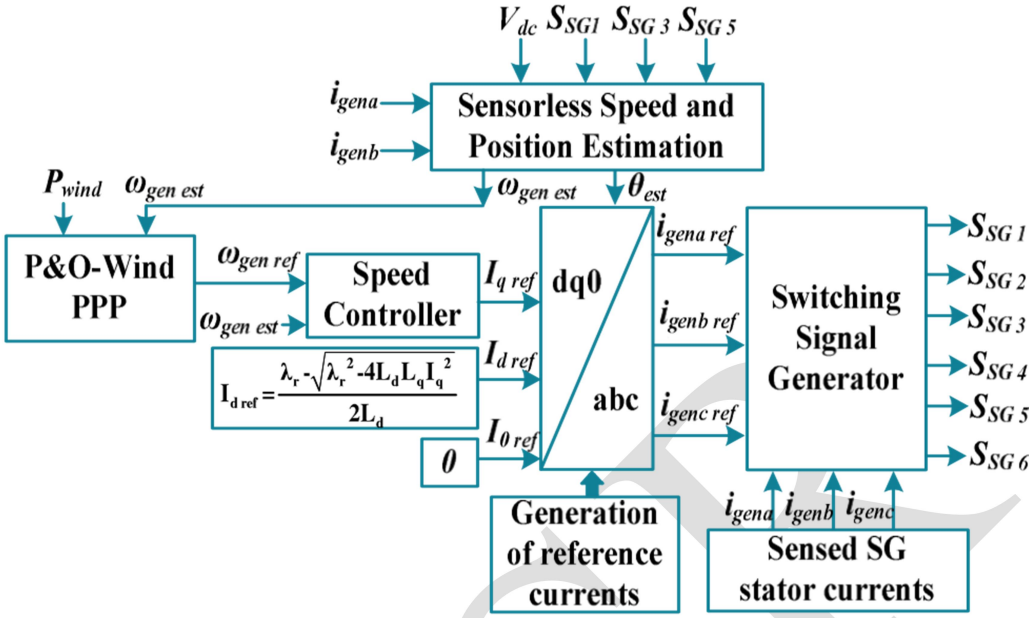

Fig. 2 Control logic of MSC.

2) Assessing the Primary Load Factor with the Help of the BC-IAPL Adaptive Filter An adaptive filter called BC-IAPL effectively generates the load's basic weight component. This adaptive filter is based on the following equation: [15],

$$w_n(k+1)=\xi\frac{\|\widetilde{u_n}(k)\widetilde{e_n}(k)\|^2}{\|\widetilde{u^T{}_n}(k)\widetilde{u_n}(k)\tilde{e}_n(k)\|^2}e_n(k)\tilde{u}_n(k)+$$
$$\xi M\beta^2{}_p\frac{\|\tilde{u}_n(k)\tilde{e}_n(k)\|^2}{\|\widetilde{u^T}_n(k)\tilde{u}_n(k)\tilde{e}_n(k)\|^2}\widehat{w_n(k)} \quad (9)$$

in which the step size is (+), the projection order is M, and >|e(k)|. When determining the margin of error,

$$e_n(k)=i_{Ln}(k)-u_n(k)w_n(k) \quad (10)$$

during each of the three phases (n=a, b, and c). By averaging the weights attained in three periods, we obtain the component (wLoad) which is supplied as

$$w_{Load}=\frac{w_a+w_b+w_c}{3} \quad (11)$$

3) Future-Focused Evaluation The dynamic responsiveness is enhanced by include the fee-forward periods of both renewable energy sources. The delivery is done in a way that

$$w_{wff}(k)=\frac{2P_{wind}(k)}{3V_t} \quad (12)$$

$$w_{pvff}(k)=\frac{2P_{pv}(k)}{3V_t} \quad (13)$$

4) Looking ahead Final Evaluation Both renewable energy sources are incorporated into the fee-forward system, which enhances its dynamic reactivity. You can think of them as

$$V_{dcref}(n)=V_{dcref}(n-1)+\Delta V_{dc};$$

$$if \begin{Bmatrix} \Delta P_{pv}>0 \; and \; \Delta V_{pv}>0 \\ \Delta P_{pv}<0 \; and \; \Delta V_{pv}<0 \end{Bmatrix} \quad (14)$$

$$V_{dref}(n) = V_{dref}(n-1) - \Delta V_{dc};$$

$$if \begin{Bmatrix} P_{pv}>0 \; and \; V_{pv}<0 \\ P_{pv}<0 \; and \; V_{pv}>0 \end{Bmatrix} \quad (15)$$

5) DC Loss Element The error of DC voltage (Vdc e) is acquired as,

$$V(n)=V(n)-V(n)_{dc\ e\ dc\ ref\ dc} \quad (16)$$

For minimization, the PI controller narrows the error. The loss component, or W_{loss}, is given as

$$w(n)=w(n-1)+k\{V(n)-V(n-1)\}+k\{V(n)\}_{loss\ loss\ il\ dc\ dc\ pl\ dc} \quad (17)$$

where, k_{il} and k_{pl} are the PI controller gains.

6) Estimation of Net Weight Constituent

Net weight is the product of all weight components, which may be expressed as: - -

$$w\ w\ www\ net\ load\ loss\ wff\ pvff = + \quad (18)$$

3.2 Generation of Utility Grid Reference Current Constituent and Switching Signal of LSC

The utility grid reference currents are estimated as, ; ;

$$ga\ ref\ a\ net\ gb\ ref\ b\ net\ gc\ ref\ c\ net\ i\ uwi\ uwi\ uw = \times = \times = \times \quad (19)$$

The LSC's gating signals (S1 through S6) are constructed using the result that is sent into the generator of switching signals. There is no difference between the reference currents (i_{ga}, i_{gb}, and i_{gc}) and the sensing currents (i_{ga}, After (i_{gb}, i_{gc})).

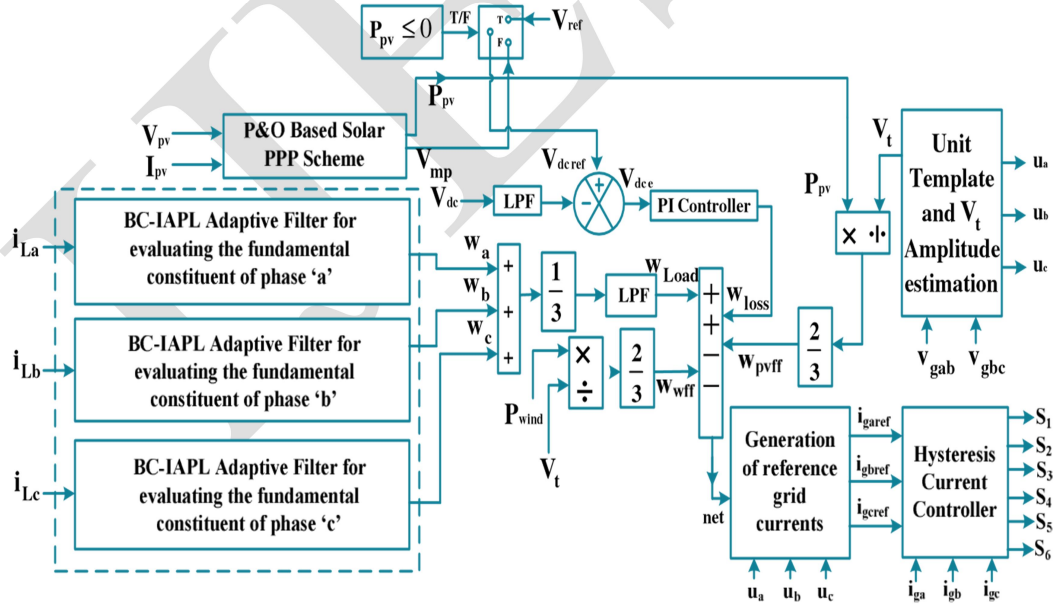

Fig. 3 LSSC Current Regulator

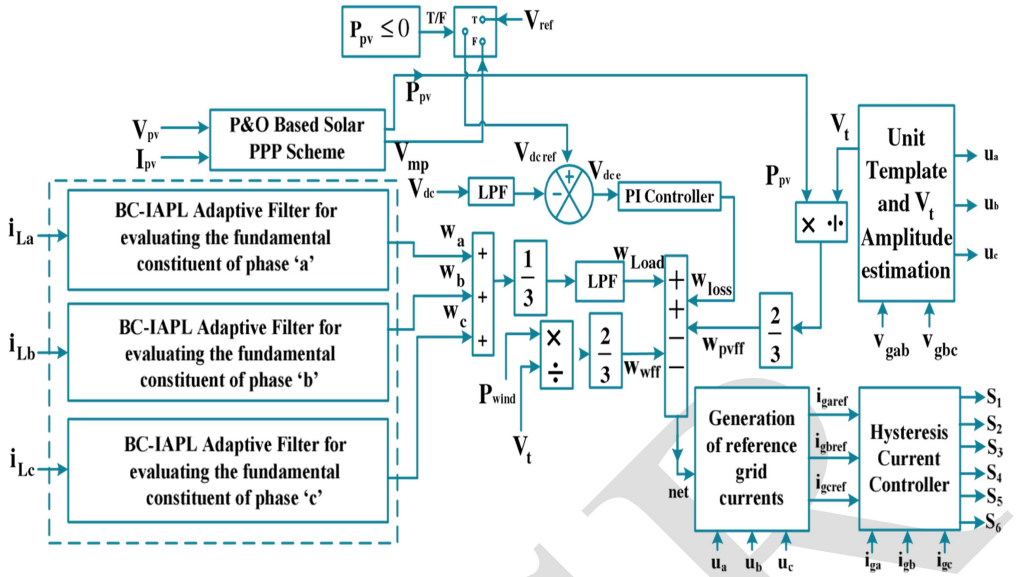

Fig 4. Fuzzy Logic based load side current control method

3.3. Fuzzy Mode Control (FMC)

Construction Planning The high-frequency oscillation and discontinuous control input that PI controllers experience greatly contribute to chattering. It is possible to construct a fuzzy controller by combining an error with a change in error. By fixing the voltage error, the Fuzzy may improve the system's performance. The FLC aims to improve the PI's learning capabilities so that the system can better withstand distortion, noise, and parameter uncertainty. The block diagram of a microgrid controlled using fuzzy logic is shown in Figure 4.

4. SIMULATED PERFORMANCE AND RESULT

We use MATLAB and Simulink to construct the microgrid model. Both on-grid and off-grid situations are taken into account. There are adjustments made to the wind speed and sun insolation as well. Using a harmonic analysis, we check the power quality indicators. Here we get into the specifics of the observed performance.

When the microgrid switches between grid-integrated and grid-isolated modes of operation, it shows the phase angles of the load voltages (V_{La}, V_{Lb}), the grid voltages (V_{ga}, V_{gb}), and the corresponding grid and load voltages (g and L). Very little changes were noticeable throughout the changeover. Therefore, the DC link voltage, together with the grid and load currents, remains constant. Regardless of the possible operational scenarios, the load is powered by electricity can observe the power consumption variations that occur when you transition from grid-integrated to grid-isolated operation. Charging batteries works in the opposite way when grid power is not available. All the while, the load demand is met and the wind power output remains within its rated amount. During the solar energy harvesting season, insolation is at its highest point. it can be observed that the microgrid transitions between grid-integrated and grid-isolated modes.

B. Strategies for Handling Wind Speed and Solar Radiation Variations and the load demonstrates the system's responsiveness to change in the velocity of the wind. The end result power of the wind generator decreases when the wind speed falls below the operating threshold. In this case, the minimum wind speed that is considered is 8 m/s, and the cut-out wind speed is 12 m/s. When the wind speed is decreased from 12 m/s to 8 m/s, the generation of wind power also decreases. The wind generator's speed is accurately controlled by the

improved sensor less speed and rotor position control. Calculates the expected and actual electrical speed of the generator, we can observe the system's response to a shift in solar insolation and the decoupling of the phase "a" load, respectively. Within specific limits, the microgrid can keep the electricity quality constant.

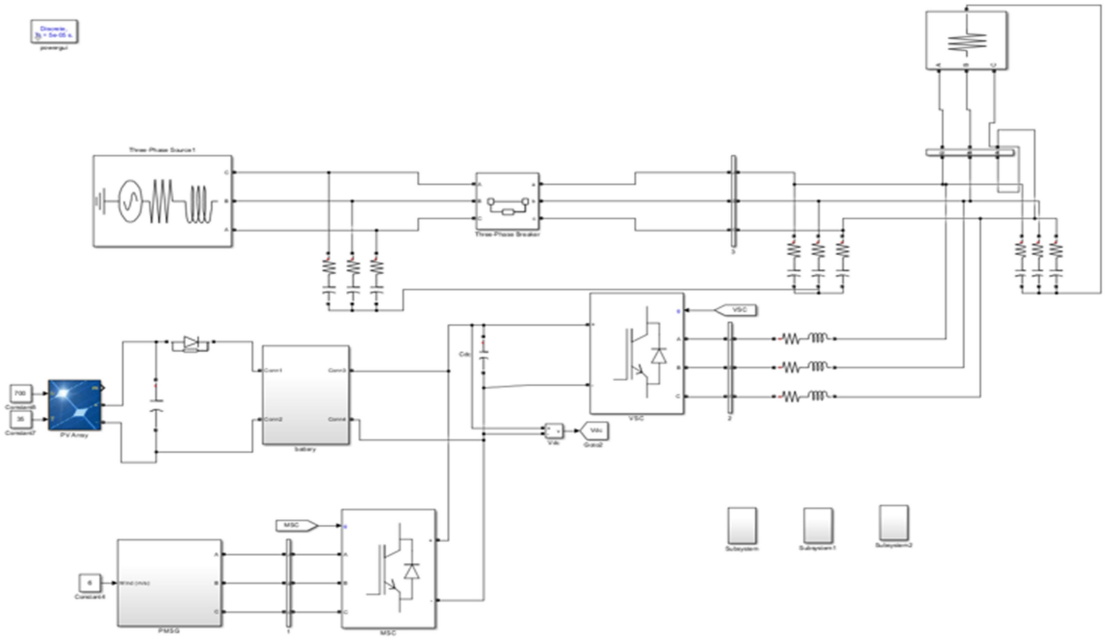

Fig 5. Simulated circuit model of pv wind dual mode grid operated system

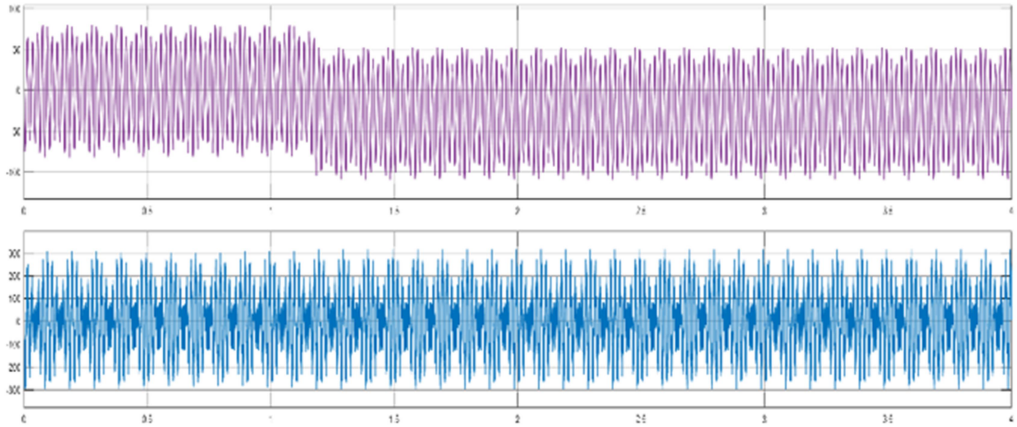

Fig 6. Grid current and voltage vs time graphs

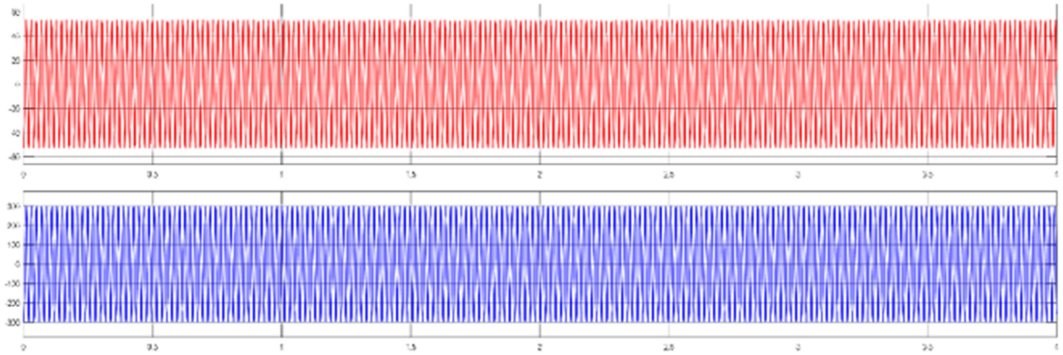

Fig 7. Load current and voltage vs time graph

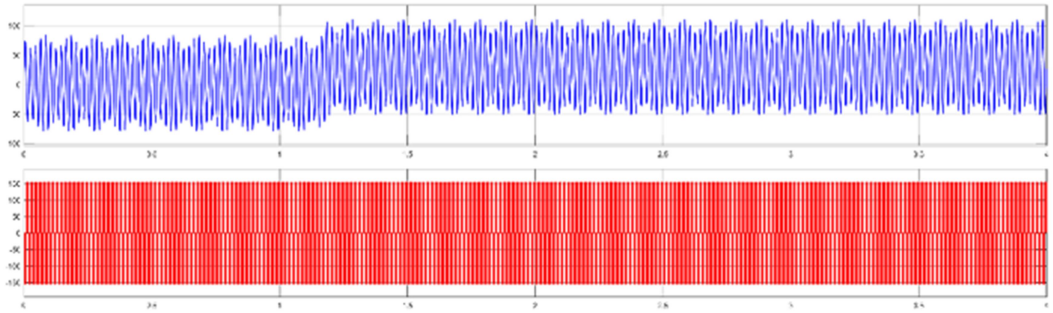

Fig 8. current and voltage vs time graph at point of common coupling

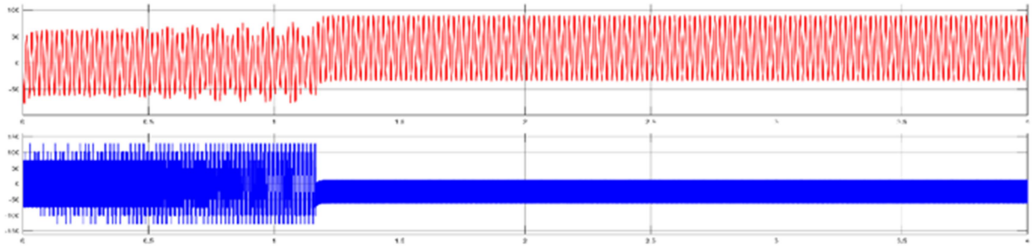

Fig 9. wind current and voltage vs time graph

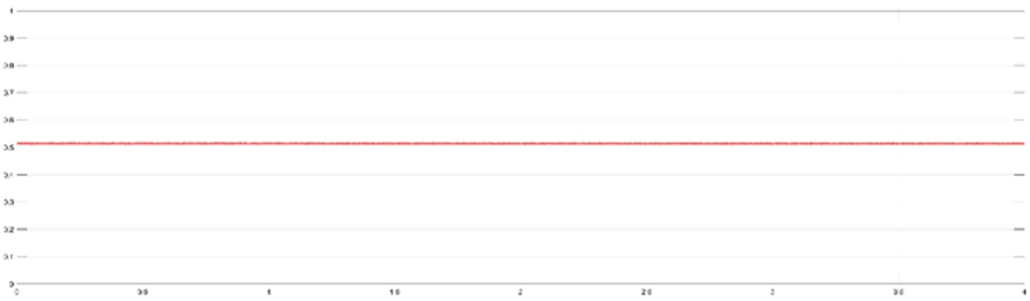

Fig 10. DC link voltage (in pu) vs time

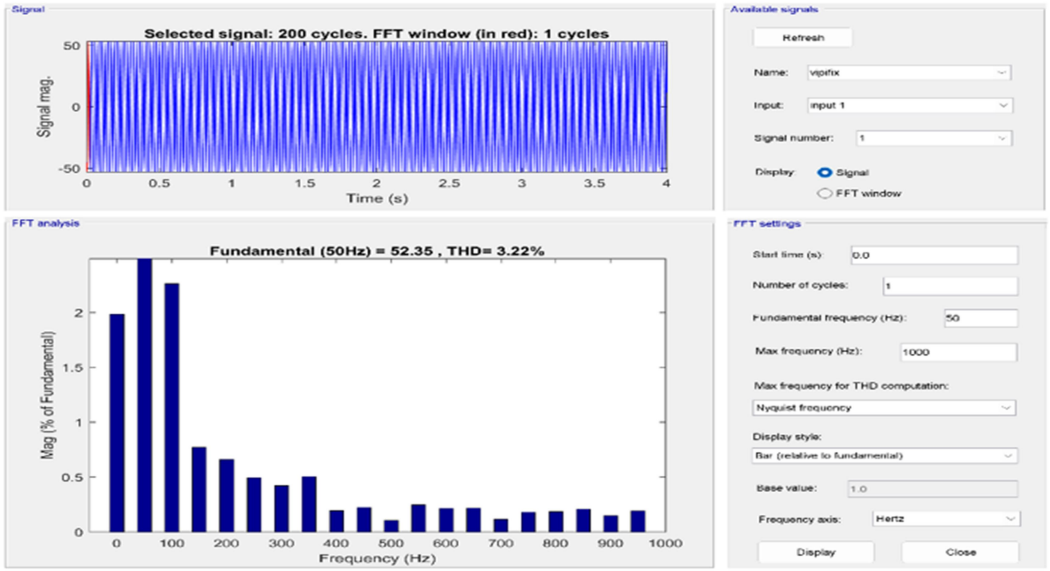

Fig 11. Load Current THD

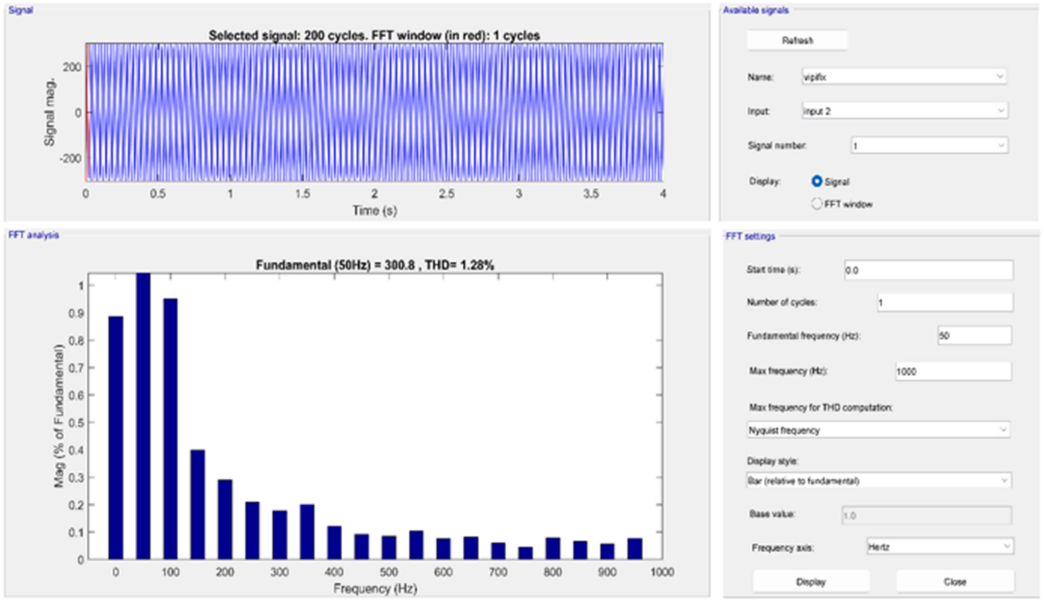

Fig 12. Load voltage THD

Table 1. THD Comparison using PI controller

Parameter	Fixed load	Variable load
Load current	3.22	4.57
Load voltage	1.27	2.27

Table 2. THD Comparison using Fuzzy controller

Parameter	Fixed load	Variable load
Load current	2.44	2.74
Load voltage	0.56	0.82

CONCLUSION

Repetitive use of the Fuzzy controller and PI can increase the microgrid system's efficiency. It has been proven that the MPR controller can successfully track AC voltage signals using DMGI-PLL. When used in current control mode, the BC-IAPL adaptive filter lowers harmonics and generates the necessary component of load currents. The voltage controller continues to function in the event of a power outage at the grid. During the seamless transition between grid-integrated and grid-isolated modes of operation, all distortions and spikes have been removed. The total harmonic distortion (THD) of the grid current is below 3%.

REFERENCES

[1] R. Khezri and A. Mahmoudi, "Review on the state-of-the-art multiobjective optimisation of hybrid standalone/grid-connected energy systems," IET Gen., Trans. Dist., vol. 14, no. 20, pp. 4285-4300, 16 10 2020.

[2] U. T. Salman, F. S. Al-Ismail and M. Khalid, "Optimal sizing of battery energy storage for grid-connected and isolated wind-penetrated microgrid," IEEE Access, vol. 8, pp. 91129-91138, 2020.

[3] A. Berrueta, A. Soto, J. Marcos, Í. de la Parra, P. Sanchis and A. Ursúa, "Identification of critical parameters for the design of energy management algorithms for li-ion batteries operating in PV power plants," IEEE Trans. Indust. Appl., vol. 56, no. 5, pp. 4670-4678, Sept.- Oct. 2020.

[4] S. Ansari, A. Chandel and M. Tariq, "A comprehensive review on power converters control and control strategies of AC/DC microgrid," IEEE Access, Early Access, 2020.

[5] IEEE Standard for Interconnection and Interoperability of Distributed Energy Resources with Associated Electric Power Systems Interfaces, IEEE Standard 1547-2018.

[6] M. Amin and Q. Zhong, "Resynchronization of distributed generation based on the universal droop controller for seamless transfer between operation modes," IEEE Trans. Indust. Elect., vol. 67, no. 9, pp. 7574- 7582, Sept. 2020.

[7] S. Yazdani, M. Ferdowsi and P. Shamsi, "Internal model based smooth transition of a three-phase inverter between islanded and gridconnected modes," IEEE Trans. Ener. Conv., vol. 35, no. 1, pp. 405- 415, March 2020.

[8] Z. Liu and J. Liu, "Indirect current control based seamless transfer of three phase inverter in distributed generation," IEEE Trans. Pow. Elect., vol. 29, no. 7, pp. 3368–3383, Jul. 2014.

[9] S. S. Thale and V. Agarwal, "Controller area network assisted grid synchronization of a microgrid with renewable energy sources and storage," IEEE Trans. Smart Grid, vol. 7, no. 3, pp. 1442–1452, 2016.

[10] Recommended Practices and Requirements for Harmonic Control on Electric Power System, IEEE Standard 519-1992, 2014.

[11] S. Kewat and B. Singh, "Improved reweighted zero-attracting quaternion-valued LMS algorithm for islanded distributed generation system at IM load," IEEE Trans. Indust. Elect., vol. 67, no. 5, pp. 3705- 3716, May 2020.

[12] P. Shah, I. Hussain and B. Singh, "Fuzzy logic based FOGI-FLL algorithm for optimal operation of single-stage three-phase grid interfaced multifunctional SECS," IEEE Trans. Indust. Inform., vol. 14, no. 8, pp. 3334-3346, Aug. 2018.

[13] F. Chishti, S. Murshid and B. Singh, "LMMN-based adaptive control for power quality improvement of grid intertie Wind–PV system," IEEE Trans. Indust. Inform., vol. 15, no. 9, pp. 4900-4912, Sept. 2019.

[14] F. Chishti, S. Murshid and B. Singh, "Frequency adaptive multistage harmonic oscillator for renewable-based microgrid under nonideal grid conditions," IEEE Trans. Indust. Elect., vol. 68, no. 1, pp. 358-369, Jan. 2021.

[15] Vasundhara, "Robust filtering employing bias compensated Mestimate affine-projection-like algorithm," Elect. Letters, vol. 56, no. 5, pp. 241-243, 5 3 2020.

[16] F. Chishti, B. Singh and S. Murshid, "Adaptive PR and BBO Based Control Strategy of Wind-Solar Integrated Standalone Microgrid for Residential Application," in Proc. IEEE Ener. Conv. Cong. Expo. (ECCE), Detroit, MI, USA, pp. 3908-3914, 2020.

[17] S. Golestan, E. Ebrahimzadeh, B. Wen, J. Guerrero and J. Vasquez, "DQ-Frame impedance modeling of three-phase grid-tied voltage source converters equipped with advanced PLLs," IEEE Trans. Pow. Elect., Early Access, 2020.

[18] F. Chishti and B. Singh, "Dual Mode Operation of Wind-Solar with Energy Storage Based Microgrid Integrated to Utility Grid," *2021 International Conference on Sustainable Energy and Future Electric Transportation (SEFET)*, Hyderabad, India, 2021, pp. 1-6